Atmos. Chem. Phys., 13, 9771–9788, 2013
www.atmos-chem-phys.net/13/9771/2013/
doi:10.5194/acp-13-9771-2013

Atmospheric Chemistry and Physics
Open Access

Validation of XCO_2 derived from SWIR spectra of GOSAT TANSO-FTS with aircraft measurement data

M. Inoue[1], I. Morino[1], O. Uchino[1], Y. Miyamoto[2], Y. Yoshida[1], T. Yokota[1], T. Machida[1], Y. Sawa[3], H. Matsueda[3], C. Sweeney[4], P. P. Tans[4], A. E. Andrews[4], S. C. Biraud[5], T. Tanaka[1,*], S. Kawakami[6], and P. K. Patra[7]

[1]National Institute for Environmental Studies (NIES), Tsukuba, Japan
[2]Graduate School of Natural Science and Technology, Okayama University, Okayama, Japan
[3]Meteorological Research Institute (MRI), Tsukuba, Japan
[4]National Oceanic and Atmospheric Administration (NOAA), Boulder, CO, USA
[5]Lawrence Berkeley National Laboratory (LBNL), Berkeley, CA, USA
[6]Japan Aerospace Exploration Agency (JAXA), Tsukuba, Japan
[7]Research Institute for Global Change, JAMSTEC, Yokohama, Japan
[*]now at: NASA Ames Research Center, Moffett Field, CA, USA

Correspondence to: M. Inoue (inoue.makoto@nies.go.jp)

Received: 30 November 2012 – Published in Atmos. Chem. Phys. Discuss.: 4 February 2013
Revised: 2 August 2013 – Accepted: 19 August 2013 – Published: 2 October 2013

Abstract. Column-averaged dry air mole fractions of carbon dioxide (XCO_2) retrieved from Greenhouse gases Observing SATellite (GOSAT) Short-Wavelength InfraRed (SWIR) observations were validated with aircraft measurements by the Comprehensive Observation Network for TRace gases by AIrLiner (CONTRAIL) project, the National Oceanic and Atmospheric Administration (NOAA), the US Department of Energy (DOE), the National Institute for Environmental Studies (NIES), the HIAPER Pole-to-Pole Observations (HIPPO) program, and the GOSAT validation aircraft observation campaign over Japan. To calculate XCO_2 based on aircraft measurements (aircraft-based XCO_2), tower measurements and model outputs were used for additional information near the surface and above the tropopause, respectively. Before validation, we investigated the impacts of GOSAT SWIR column averaging kernels (CAKs) and the shape of a priori profiles on the aircraft-based XCO_2 calculation. The differences between aircraft-based XCO_2 with and without the application of GOSAT CAK were evaluated to be less than ± 0.4 ppm at most, and less than ± 0.1 ppm on average. Therefore, we concluded that the GOSAT CAK produces only a minor effect on the aircraft-based XCO_2 calculation in terms of the overall uncertainty of GOSAT XCO_2.

We compared GOSAT data retrieved within ± 2 or $\pm 5°$ latitude/longitude boxes centered at each aircraft measurement site to aircraft-based data measured on a GOSAT overpass day. The results indicated that GOSAT XCO_2 over land regions agreed with aircraft-based XCO_2, except that the former is biased by -0.68 ppm (-0.99 ppm) with a standard deviation of 2.56 ppm (2.51 ppm), whereas the averages of the differences between the GOSAT XCO_2 over ocean and the aircraft-based XCO_2 were -1.82 ppm (-2.27 ppm) with a standard deviation of 1.04 ppm (1.79 ppm) for $\pm 2°$ ($\pm 5°$) boxes.

1 Introduction

Global warming has become a serious international environmental issue over the last few decades. Forecasting concentrations of carbon dioxide (CO_2), which is the most important anthropogenic greenhouse gas (GHG), is required to predict the magnitude of global warming and future climate conditions. Atmospheric CO_2 concentrations have been measured with high accuracy at ground stations and tall towers as well as on ships, aircraft, and balloons using flask sampling or continuous measurement equipment. These measurements have provided extensive information regarding the latitudinal distribution and temporal variations of CO_2 in the atmosphere (e.g., Pales and Keeling, 1965; Conway et al., 1988;

Published by Copernicus Publications on behalf of the European Geosciences Union.

Komhyr et al., 1989; Tans et al., 1989; Inoue and Matsueda, 1996; Nakazawa et al., 1997b; Watanabe et al., 2000; Matsueda et al., 2002; Machida et al., 2008; Sawa et al., 2008). Atmospheric measurements have also provided reasonable estimates of the global land-ocean partitioning or latitudinal distributions of surface fluxes of CO_2 through inverse modeling (Enting, 2002). However, because of the sparseness of existing observation sites and the limitations of their altitudinal range, current estimates of regional CO_2 sources and sinks have large uncertainties (Gurney et al., 2002).

Recently, a great deal of attention has been given to CO_2 observations using satellite remote sensing technology that can identify the regional distribution of GHGs and estimate their emissions and absorptions at the subcontinental scale. Rayner and O'Brien (2001) reported that the uncertainty in CO_2 fluxes estimated by inverse modeling can be substantially reduced if the current surface network is supplemented by spaceborne measurements of CO_2 column-averaged concentrations provided that individual column concentrations achieved a precision within $\pm 1\,\%$ without bias or with uniform bias. Although GHG observation by satellites has the advantage that the whole globe can be observed by a single instrument, it is considered to be less accurate than ground-based measurement (e.g., Christi and Stephens, 2004). Therefore, satellite-based data products must be validated by higher-precision data obtained independently such as ground-based Fourier transform spectrometer (FTS) data and aircraft measurement data.

Here, we present a brief overview of the current situation regarding GHG observations using satellite remote sensing. The temporal variations of CO_2 concentrations have been observed with the High-Resolution Infrared Sounder (HIRS; Chédin et al., 2002) onboard the National Oceanic and Atmospheric Administration (NOAA) polar meteorological satellites and the Atmospheric Infrared Sounder (AIRS; Crevoisier et al., 2004) onboard the Aqua satellite platform of the National Aeronautics and Space Administration (NASA). The SCanning Imaging Absorption spectroMeter for Atmospheric CHartographY (SCIAMACHY) instrument onboard ENVISAT, launched in March 2002 and operated until April 2012, made nadir observations in the near-infrared of the main GHGs and the ozone precursor gases (Dils et al., 2006). Column-averaged dry air mole fractions of carbon dioxide (XCO_2) derived from the SCIAMACHY instrument have been compared to ground-based FTS data (Dils et al., 2006; Schneising et al., 2012; Heymann et al., 2012).

More recently, the Greenhouse gases Observing SATellite (GOSAT), the world's first satellite dedicated to measuring the atmospheric concentrations of CO_2 and CH_4 from space, has been operated since the early 2009, and observational results have been reported (Yokota et al., 2009; Yoshida et al., 2011; Morino et al., 2011; Oshchepkov et al., 2013). Yoshida et al. (2013) presented global distributions of XCO_2 retrieved from the Short-Wavelength InfraRed (SWIR) spectra of the Thermal And Near-infrared Sensor for carbon Observation-Fourier Transform Spectrometer (TANSO-FTS) onboard the GOSAT. In addition, they performed the validation of GOSAT SWIR XCO_2 (ver. 02.xx, latest version released in June 2012) with data provided by a worldwide network of ground-based FTS called the Total Carbon Column Observing Network (TCCON, Wunch et al., 2011) and showed that the mean bias of the GOSAT XCO_2 (ver. 02.xx) was -1.48 ppm with a standard deviation of 2.09 ppm.

Along with the TCCON data, aircraft measurement data are useful for the validation of the satellite data. Araki et al. (2010) showed that the uncertainty of XCO_2 over Tsukuba calculated using aircraft data at one aircraft measurement site of Narita was estimated to be $\sim$1 ppm and calculating XCO_2 from airliners could be applied to the validation of GOSAT products. In addition, Miyamoto et al. (2013) provided a method to calculate XCO_2 based on aircraft measurement vertical data (hereinafter aircraft-based XCO_2) at various locations over the world. In this study, we validated ver. 02.00 of the GOSAT SWIR XCO_2 with the aircraft-based XCO_2 calculated using the method as in Miyamoto et al. (2013). This paper is organized as follows: in Sect. 2, we describe GOSAT products, the aircraft measurements and meteorological tower data used in this study. In Sect. 3, the methodology used for the analysis is provided. In Sect. 4, the impacts of GOSAT SWIR column averaging kernels (CAKs) and assumed profiles in the stratosphere and mesosphere on aircraft-based XCO_2 calculation are examined. Then, comparisons between GOSAT products and aircraft-based XCO_2 are performed. We conclude the paper with a summary in Sect. 5.

2 Observations

2.1 Overview of GOSAT and products retrieved from GOSAT TANSO-FTS SWIR spectra

GOSAT is a satellite for spectroscopic remote sensing of the greenhouse gases that was launched on 23 January 2009 (Kuze et al., 2009). TANSO-FTS, onboard GOSAT, has three bands in the SWIR region centered at 0.76, 1.6, and 2.0 µm and one broad thermal infrared (TIR) band between 5.6 and 14.3 µm. The measurements in SWIR and TIR bands allow for the retrievals of XCO_2 and CO_2 concentration profiles, respectively (Saitoh et al., 2009; Yoshida et al., 2011, 2013). In this study, we performed the validation of XCO_2 retrieved from SWIR spectra with the latest retrieval algorithm (ver. 02.xx; see Yoshida et al., 2013, for details). Validation of the GOSAT TANSO-FTS SWIR level 2 products is of great significance, because these data form the basis of level 3 (data on the global distribution of XCO_2) and level 4 products (GHG fluxes). Level 2 products are already in use as part of the observational data to estimate surface CO_2 fluxes by inverse modeling and data assimilation (e.g., Takagi et al., 2011; Maksyutov et al., 2013; Saeki et al., 2013). Therefore,

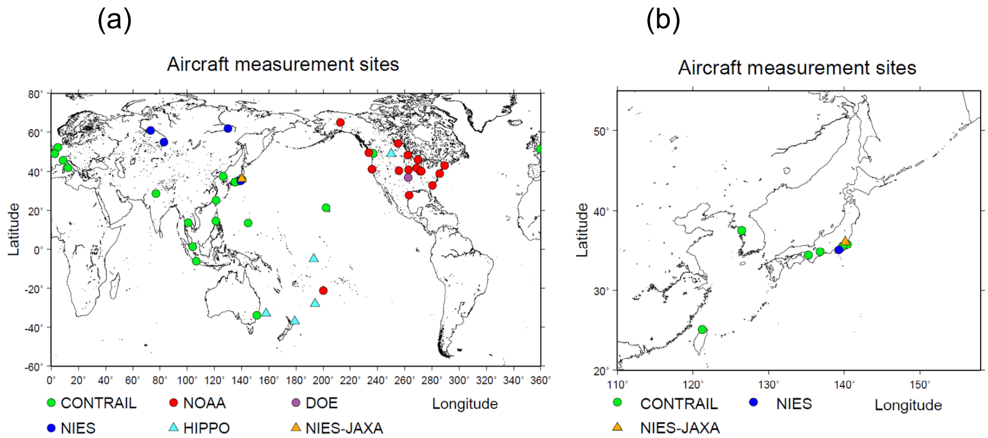

Fig. 1. (a) Location of aircraft observation sites used for GOSAT validation. The East Asian region is expanded in **(b)**.

GOSAT level 2 products (ver. 02.00 released in June 2012) must be evaluated using independent data with higher precision and no significant bias, i.e., a very small uncertainty. Here, we compare the GOSAT SWIR XCO_2 with aircraft-based XCO_2.

2.2 Aircraft measurement data

The CONTRAIL project has started since late 2005 and been observing vertical CO_2 profiles using Japan Airlines Corporation (JAL) commercial airliners (Machida et al., 2008; Matsueda et al., 2008), which record frequent and spatially dense observation data. Five JAL commercial aircraft were instrumented with continuous CO_2 measuring equipment (CME), and most flights originate from Narita International Airport (hereinafter Narita) in Chiba, Japan. The data observed during the ascent and descent of the aircraft are taken as vertical CO_2 profiles over each observation site (airport), and have an overall uncertainty of 0.2 ppm. Typical observing altitudes are 1–11 km with vertical resolutions of 30–100 m. The CONTRAIL data are being used to gain an understanding of the meridional and seasonal variations of CO_2 near the tropopause (Sawa et al., 2008) and to validate or estimate CO_2 fluxes by inverse modeling for Asian regions (Patra et al., 2011; Niwa et al., 2012). The vertical CO_2 profiles are used in this study.

The NOAA Earth System Research Laboratory/Global Monitoring Division (ESRL/GMD) operates an aircraft-based flask air-sampling network designed to monitor the global distribution and interannual variations of CO_2 and several other trace gases in the atmosphere (NOAA/ESRL Carbon Cycle Greenhouse Gases Aircraft Program). Several atmospheric gases including CO_2 are measured using aircraft at about 20 sites, covering an altitude range of ∼500 m to 7 km with vertical resolutions of 300–700 m, at weekly or biweekly sampling intervals. The measurement uncertainty is reported to be ∼0.15 ppm. The NOAA ESRL/GMD aircraft measurements have been used for the validation of AIRS CO_2 retrieval at various pressure levels (Maddy et al., 2008).

The US Department of Energy (DOE) supports an aircraft-based observation program in the Southern Great Plains (SGP) as part of a joint effort between the Atmospheric Radiation Measurement (ARM) program, NOAA/ESRL, and the Lawrence Berkeley National Laboratory ARM Carbon project (Biraud et al., 2013). Flasks are collected approximately twice per week by small aircraft (Cessna 172 initially, then Cessna 206) on a series of horizontal legs ranging in altitude from 460 m to 5.5 km, and analyzed by NOAA/ESRL for a suite of carbon cycle gases and isotopes, thereby linking all flights to the global cooperative air-sampling network.

NIES also measures CO_2 densities by flask air sampling using aircraft to examine vertical and horizontal distributions of GHGs. There are three sites in Siberia and one site in Japan. Sampling frequency is once or twice a month. Typical observing altitudes are 0.5–7 km with vertical resolutions of 0.5–1.5 km, and the uncertainty of measurements is estimated to be 0.2 ppm, including the scale difference between standard gases (Nakazawa et al., 1997c; Machida et al., 2001).

Aircraft measurements obtained by the HIAPER Pole-to-Pole Observations (HIPPO) are also available for the GOSAT validation. The HIPPO project is a sequence of five global aircraft measurement programs that sample and measure the atmosphere from the North Pole through the coastal waters of Antarctica in the Pacific Basin, spanning the seasons (Wofsy et al., 2011). Most profiles extended from approximately 0.3 to 8.5 km altitudes, but sometimes above approximately 14 km. We here utilized the 10 s merged CO_2 data obtained from the second and third HIPPO missions (HIPPO-2 and HIPPO-3), which took place from October to November 2009 and from March to April 2010, respectively (Wofsy et al., 2012).

In addition, the NIES and the Japan Aerospace Exploration Agency (JAXA) jointly make aircraft measurements of CO_2 and CH_4 over Japan about once or twice a year (hereinafter NIES-JAXA campaign). In this study, we used CO_2 profiles over Tsukuba (36.1° N, 140.1° E) in February 2010 obtained by flask sampling whose analytical precision is better than 0.03 ppm (Tanaka et al., 2012). However, the flight over Tsukuba was restricted to altitudes below 2 km because of the controlled airspace for the two international airports. Therefore, the altitudes from 7 to 2 km were sampled over Kumagaya (36.1° N, 139.2° E), about 70 km west of Tsukuba. Vertical profiles measured at Kumagaya and Tsukuba were used in the calculation of XCO_2 at Tsukuba. More detail is given in Tanaka et al. (2012).

There are other regular aircraft measurements or campaigns over the world. We also investigated data obtained from the TCCON calibration campaign in Europe (Wunch et al., 2010; Messerschmidt et al., 2011). Unfortunately, there were no data temporally matched up with the GOSAT data at European sites. Additionally, an observational altitude of regular aircraft measurements at the Bialystok site is restricted to about 3 km (Messerschmidt et al., 2012). Since it is very difficult to calculate XCO_2 without large uncertainties, CO_2 profiles at Bialystok were not used in this study.

In this study, 20 CONTRAIL sites, 16 NOAA sites, 1 DOE site, 4 NIES sites, 2 missions of HIPPO, and 1 NIES-JAXA campaign site were used for validation of GOSAT products. The respective locations are shown in Fig. 1, and their basic information is given in Table 1. CONTRAIL sites are widely distributed around the world, including Asia, Oceania, and Europe, whereas NOAA sites are concentrated mainly in North America (Fig. 1).

2.3 Tower data

The aircraft measurement data are obtained over a limited altitude range (about 0.5–12 km above the surface). As for additional information below the lower boundary of the aircraft data, we use the CO_2 concentration data measured by the tall towers of the Meteorological Research Institute (MRI) and NOAA. Because there are tall towers at limited aircraft measurement sites, four aircraft sites can use tower data: NRT and TKB use MRI tower data, and LEF and WBI use NOAA tower data (see Table 1 for site code of aircraft sites).

CO_2 concentrations were observed at a meteorological tower in the MRI, Tsukuba, Japan (36.1° N, 140.1° E, Inoue and Matsueda, 1996, 2001). Atmospheric concentrations of CO_2 at altitudes of 1.5, 25, 100, and 200 m above the ground were continuously observed with a precision better than 0.1 ppm using a non-dispersive infrared (NDIR) analyzer (Inoue and Matsueda, 1996) and recorded as hourly data. The tower data nearest to the aircraft measurement time were selected to complement CO_2 profiles.

The NOAA ESRL/GMD tall tower network also provides representative measurements of CO_2 in the continental boundary layer (Andrews et al., 2011). CO_2 data from two NOAA tower sites – Park Falls (Wisconsin, USA) and West Branch (Iowa, USA) – were used for LEF and WBI, respectively. There are three main observation stages: 30, 122, and 396 m above the ground in Park Falls, and 31, 99, and 379 m above the ground in West Branch. Observations were made several times over 10 min periods and every 30 s for the highest altitudes. We used averages of the data obtained within ±10 min of the beginning of the profile sampling time by the aircraft at each altitude to calculate XCO_2.

3 Analysis methods

3.1 XCO_2 calculation from aircraft data

The XCO_2 calculation method from aircraft data in this study was equivalent to that described previously by Miyamoto et al. (2013). Due to the limited range of altitudes for aircraft measurements, further observational data or certain assumptions were required near the surface and in the middle atmosphere. In the following subsections, we show a brief summary to construct a CO_2 profile from aircraft measurements as well as tower and model data.

3.1.1 Tropospheric profiles and the tropopause height

CO_2 profiles in the troposphere were constructed in a manner similar to that described by Araki et al. (2010). Where tower data were available, they were used near the surface to complement the CO_2 profiles of aircraft-based data. Where there were no tower data for a site, we extrapolated profiles obtained by the aircraft to the surface from the lowest measured aircraft data. When an airliner did not fly above the tropopause, the CO_2 concentration at the highest observational altitude was assumed to be constant up to the tropopause. The local tropopause height was determined from the Global Forecast System (GFS) model (http://nomads.ncdc.noaa.gov/) produced by the National Centers for Environmental Prediction (NCEP), and was in good agreement with radiosonde measurements (Pan and Munchak, 2011). In this study, we used the GFS tropopause height data provided as reanalysis values at 00:00, 06:00, 12:00, and 18:00 UTC, and the forecast values at 03:00, 09:00, 15:00, and 21:00 UTC (3 h after the reanalysis time) with $1° \times 1°$ horizontal grids. For aircraft profiles that were measured higher than the local tropopause, model outputs in the stratosphere (see Sect. 3.1.2) were added above the highest aircraft measurement.

3.1.2 Profiles of the stratosphere and mesosphere

To complete stratospheric and mesospheric profiles, Araki et al. (2010) used an empirical model of profiles at midlatitudes in the Northern Hemisphere. We used profiles derived from the mean "age of air," defined as the time required for an air parcel to transit from the Earth's surface to the layers above (Kida, 1983), at various altitudes according to

Table 1. Basic information for the aircraft measurement sites used for the GOSAT validation.

(a) CONTRAIL

site code	latitude [deg. N]	longitude [deg. E]	elevation [m]	region	airport name
AMS	52.3	4.8	3	Amsterdam	Schiphol Airport
LHR	51.5	−0.5	24	London	Heathrow Airport
YVR	49.2	−123.2	4	Vancouver	Vancouver International Airport
CDG	49.0	2.5	119	Paris	Charles de Gaulle International Airport
MXP	45.6	8.7	24	Milan	Milan Malpensa International Airport
FCO	41.8	12.3	5	Rome	Fiumicino Airport
ICN	37.5	126.5	7	Incheon	Incheon International Airport
NRT	35.8	140.4	43	Narita	Narita International Airport
HND	35.6	139.8	6	Haneda	Tokyo International Airport
NGO	34.9	136.8	5	Nagoya	Chubu Centrair International Airport
KIX	34.4	135.2	0	Kansai	Kansai International Airport
DEL	28.6	77.1	237	Delhi	Indira Gandhi International Airport
TPE	25.1	121.2	32	Taipei	Taiwan Taoyuan International Airport
HNL	21.3	−157.9	4	Honolulu	Honolulu International Airport
MNL	14.5	121.0	23	Manila	Ninoy Aquino International Airport
BKK	13.7	100.7	2	Bangkok	Suvarnabhumi International Airport
GUM	13.5	144.8	91	Guam	Guam International Airport
SIN	1.4	104.0	7	Singapore	Singapore Changi International Airport
CGK	−6.1	106.7	10	Jakarta	Jakarta International Soekarno-Hatta Airport
SYD	−33.9	151.2	6	Sydney	Kingsford Smith Airport

(b) NOAA

site code	latitude [deg. N]	longitude [deg. E]	elevation [m]	region	site name
PFA	65.1	−147.3	210	United States	Poker Flat, Alaska
BRM	54.3	−105.0	507	Canada	BERMS, Saskatchewan
ESP	49.6	−126.4	7	Canada	Estevan Point, British Columbia
DND	48.4	−97.8	464	United States	Dahlen, North Dakota
LEF	45.9	−90.3	472	United States	Park Falls, Wisconsin
NHA	43.0	−70.6	0	United States	Worcester, Massachusetts
WBI	41.7	−91.4	242	United States	West Branch, Iowa
THD	41.1	−124.2	107	United States	Trinidad Head, California
BNE	40.8	−97.2	466	United States	Beaver Crossing, Nebraska
CAR	40.4	−104.3	1740	United States	Briggsdale, Colorado
HIL	40.1	−87.9	202	United States	Homer, Illinois
AAO	40.1	−88.6	213	United States	Airborne Aerosol Observing, Illinois
CMA	38.8	−74.3	0	United States	Cape May, New Jersey
SCA	32.8	−79.6	0	United States	Charleston, South Carolina
TGC	27.7	−96.9	0	United States	Sinton, Texas
RTA	−21.3	−159.8	3	Cook Islands	Rarotonga

(c) DOE

site code	latitude [deg. N]	longitude [deg. E]	elevation [m]	region	site name
SGP	36.8	−97.5	314	United States	Southern Great Plains, Oklahoma

(d) NIES

site code	latitude [deg. N]	longitude [deg. E]	elevation [m]	region	site name
YAK	62	130	136	Russia	Yakutsk
SUR	61	73	35	Russia	Surgut
NOV	55	83	143	Russia	Novosibirsk
SGM	35.1	139.3	0	Japan	Sagami-bay

(e) HIPPO

site code	latitude [deg. N]	longitude [deg. E]	elevation [m]	region	site name
HPA	49	−110	1040	United States	northeastern part of Great Falls, Montana
HPB	−28	−166	0	South Pacific Ocean	southeastern part of Tonga
HPC	−33	158	0	Australia	eastern part of Lord Howe
HPD	−5	−167	0	Kiribati	western part of Enderbury
HPE	−37	179	0	New Zealand	northeastern part of Bay of Plenty

(f) NIES−JAXA campaign

site code	latitude [deg. N]	longitude [deg. E]	elevation [m]	region	site name
TKB	36.1	140.1	31	Japan	Tsukuba

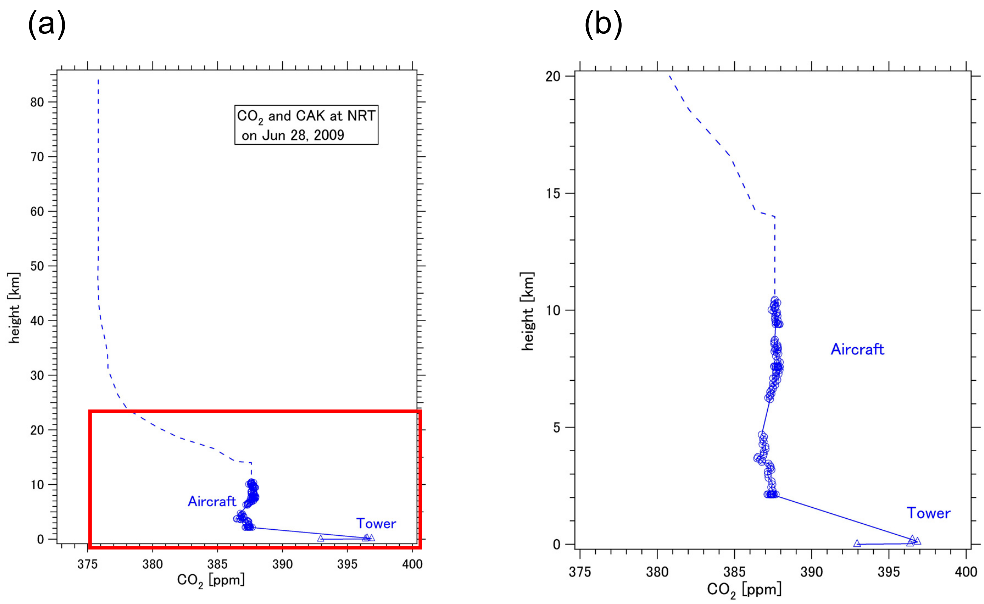

Fig. 2. An example of CO_2 profiles constructed over Narita (Japan). **(a)** High-altitude profile. The red rectangular area is expanded in **(b)**. The open circles and triangles represent aircraft data and tower data, respectively. The solid and dashed lines show the observed and assumed CO_2 profiles, respectively. See the text for more details.

the method described by Miyamoto et al. (2013) in order to apply the method of Araki et al. (2010) to the XCO_2 calculation at various regions. The age of air was determined from the Center for Climate System Research/National Institute for Environmental Studies/Frontier Research Center for Global Change (CCSR/NIES/FRCGC) atmospheric-general-circulation-model (AGCM, Numaguti et al., 1997)-based chemical transport model (referred to as the ACTM, Patra et al., 2009). The age was converted to a CO_2 mixing ratio by assuming a tropospheric concentration (corresponding to a 0 yr old mixing ratio) in 2006 of 381.2 ppm and an annual trend of 1.9 ppm yr^{-1} at every site (WMO, 2007). The actual global mean CO_2 concentration in 2009 was 386.8 ppm (WMO, 2010), and the actual mean annual trend during the period 2006–2009 was approximately 1.9 ppm yr^{-1}. The vertical structure of the CO_2 concentration estimated by the age of air was consistent with balloon measurements of CO_2 over Japan (Nakazawa et al., 1995; Miyamoto et al., 2013). Although ACTM was used for profiles of the stratosphere and mesosphere in this study, we evaluated the impact of profiles in the middle atmosphere on the aircraft-based XCO_2 calculation using the two other model outputs discussed in Sect. 4.2.

3.1.3 Dry air number density profiles

To obtain the number density profiles of dry air, we utilized meteorological data from the Committee on Space Research (COSPAR) International Reference Atmosphere (CIRA-86; Fleming et al., 1990), which provides empirical models of atmospheric temperature and air number densities from the surface to 120 km. We estimated the aircraft-based XCO_2 using the air number densities of CIRA-86 and grid point value (GPV) data from a numerical weather prediction model developed by the Japan Meteorological Agency (e.g., Nakakita et al., 1996). The aircraft-based XCO_2 data where air number densities of GPV were used below 10 hPa and CIRA-86 above 10 hPa (GPV-CIRA XCO_2) were compared to values calculated using the CIRA-86 data vertically throughout the atmosphere (CIRA XCO_2). We estimated an average of 113 cases obtained at the Narita site in 2009. The results showed that an average and ±1 standard deviation (1σ) of the differences between "CIRA XCO_2" and "GPV-CIRA XCO_2" were as small as 0.0005 ± 0.0326 ppm. In addition, Araki et al. (2010) also indicated that the XCO_2 calculated by air number densities of CIRA-86 was in agreement with values calculated from a rawinsonde over Tsukuba to within 0.08 ppm. Therefore, we used the air number densities obtained solely by CIRA-86 as the air number densities of dry air in this study.

3.1.4 Aircraft-based CO_2 profiles and XCO_2 with and without column averaging kernel (CAK)

An example of aircraft-based CO_2 profiles is shown in Fig. 2. The open circles and triangles represent aircraft measurement data and tower data, respectively. In addition, the solid and dashed lines show the observed (i.e., based on in situ measurements) and assumed CO_2 profiles, respectively. Based on aircraft-based CO_2 profiles, XCO_2 with and without applying GOSAT SWIR CAK is calculated.

CAK $\boldsymbol{a}$ is defined as

$$a_j = (\boldsymbol{h}^T \mathbf{A})_j \frac{1}{h_j}, \quad (1)$$

where the subscript j denotes the index of the j-th layer, $\mathbf{A}$ is the averaging kernel matrix, and $\boldsymbol{h}$ is a pressure weighting function calculated based on the dry air number density profile (Connor et al., 2008; Ohyama et al., 2009; Yoshida et al., 2010). CAK is a function of pressure and solar zenith angle. The GOSAT CAKs with respect to solar zenith angle are shown in Fig. S1 in the Supplement. The XCO_2 values for the aircraft profile that is weighted by the CO_2 CAK $\boldsymbol{a}$ are calculated according to the method of Rodgers and Connor (2003) and Connor et al. (2008).

$$X_{CO_2}^{\text{in-situ,CAK}} = X_{CO_2}^{a} + \sum_j h_j a_j \left(t_{\text{in-situ}} - t_{\text{a}}\right)_j \quad (2)$$

$$= \boldsymbol{h}^T \left[\mathbf{A} \cdot \boldsymbol{t}_{\text{in-situ}} + (\mathbf{I} - \mathbf{A})\, \boldsymbol{t}_{\text{a}}\right] \quad (3)$$

where $X_{CO_2}^{a}$ is the column-averaged dry air mole fractions of CO_2 for the a priori profile $\boldsymbol{t}_{\text{a}}$, and $\boldsymbol{t}_{\text{in-situ}}$ is the aircraft-based CO_2 profile. The a priori CO_2 profile for GOSAT is calculated for every observation day by an offline global atmospheric transport model developed by NIES (NIES TM, Maksyutov et al., 2008). GOSAT a priori profiles have some effects on XCO_2 retrieval.

Aircraft-based XCO_2 without applying the CO_2 CAK can be expressed as

$$X_{CO_2}^{\text{in-situ,noCAK}} = \boldsymbol{h}^T \cdot \boldsymbol{t}_{\text{in-situ}}. \quad (4)$$

Note that the actual altitudinal integrations of Eqs. (3) and (4) were conducted from the ground up to the altitude of the mesopause (∼85 km) with a vertical resolution of 100 m based on the method described by Araki et al. (2010). Based on the method of Miyamoto et al. (2013), we calculated the uncertainty of aircraft-based XCO_2 for each flight. In this study, we use the aircraft-based XCO_2 data with an uncertainty of less than 1 ppm for validation of GOSAT XCO_2 data. Detail of the uncertainty is described in Miyamoto et al. (2013).

It is necessary to apply the GOSAT SWIR CAK and convolution with the a priori profiles used in satellite data retrievals to the aircraft measurement data for a meaningful comparison between the two measurements. We applied the GOSAT CAK to aircraft-based XCO_2 calculation when comparing the GOSAT data with temporally matched aircraft data (Sect. 4.3). On the other hand, we cannot apply the GOSAT SWIR CAK to the fitted aircraft-based XCO_2 due to the absence of the vertical information for all aircraft measurements when comparing of GOSAT SWIR XCO_2 with the gap-filling time series of the aircraft-based XCO_2 through curve fitting (see the Supplement for details on comparisons by the curve fitting method). Therefore, we first evaluated the impact of GOSAT SWIR CAK on the aircraft-based XCO_2 calculation (Sect. 4.1).

3.2 Validation method for GOSAT products using aircraft data

Based on the results of the impacts of GOSAT SWIR CAK on the XCO_2 calculation, we performed a comparison of the GOSAT data retrieved within ±2 or ±5° latitude/longitude boxes centered at each observation site and aircraft-based data measured on a GOSAT overpass day. The aircraft data temporally nearest to the GOSAT overpass time were selected where there were multiple aircraft data associated with the particular GOSAT data. Scatter diagrams between GOSAT XCO_2 and aircraft-based XCO_2 are presented for land and ocean separately, and correlation coefficients and their differences are estimated in Sect. 4.3.

This extraction method enabled us to validate GOSAT products using the temporally matched observational data. However, this method resulted in no temporally matched data at certain observation sites where no aircraft measurements were made on the GOSAT overpass day. Therefore, we compared GOSAT XCO_2 with temporally interpolated aircraft-based XCO_2 data by curve fitting (e.g., Nakazawa et al., 1997a) in the Supplement.

4 Results

4.1 Impact of GOSAT SWIR CAK on the aircraft-based XCO_2 calculation

The impact of the GOSAT SWIR CAK on the aircraft-based XCO_2 calculation was evaluated for each observation site. We made a connection between aircraft-based data at a certain time of the day and the GOSAT data nearest to the aircraft observation site for all GOSAT data obtained within ±10° latitude/longitude boxes centered at the observation site on the same day. When we use the ±5° boxes, the number of unavailable observation site becomes more than 10, and the results for available sites are almost same as those for the ±10° boxes (results for the ±5° boxes are not shown). In this study, XCO_2 calculated from the aircraft-based data weighted with a selected GOSAT SWIR CAK using Eq. (2) was expressed as “aircraft-based XCO_2 with CAK,” whereas XCO_2 calculated from the aircraft-based data without the application of GOSAT CAK using Eq. (4) was expressed as “aircraft-based XCO_2 without CAK.”

Before evaluation of the GOSAT CAK impacts, we show examples of vertical profiles of CO_2 densities and CAK over several locations. In Fig. 3a and b, black lines, blue open circles, and blue triangles indicate the GOSAT SWIR CAK and profiles of the aircraft and tower measurements of CO_2 over Narita, respectively. Red lines indicate the GOSAT a priori profiles of CO_2, which were calculated for the day of observation by NIES TM. The atmosphere was divided into 15 layers from the surface to 0.1 hPa with a constant pressure difference. We focused on 28 June 2009 (Fig. 3a),

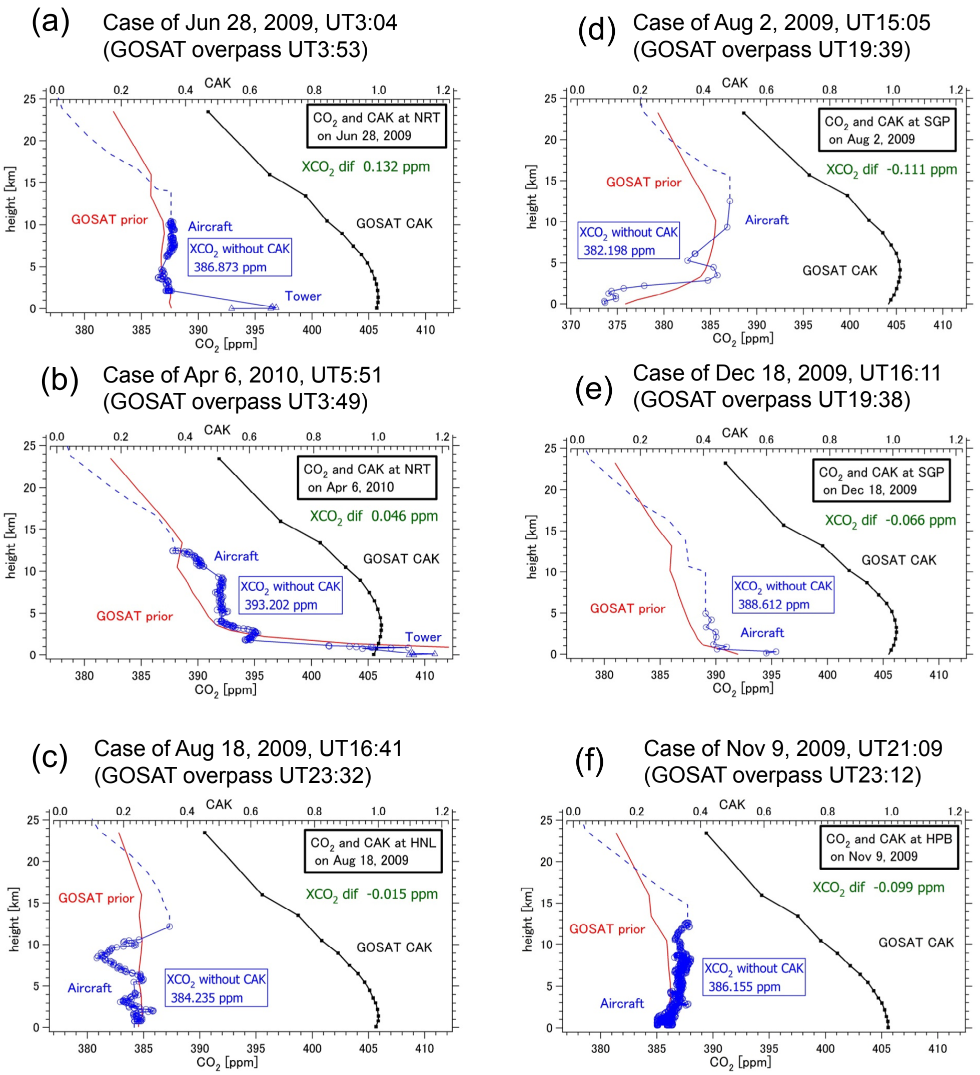

Fig. 3. Vertical profiles of CO_2 and GOSAT CAK over Narita on **(a)** 28 June 2009 and **(b)** 6 April 2010, over **(c)** Honolulu on 18 August 2009, over the Southern Great Plains on **(d)** 2 August 2009 and **(e)** 18 December 2009, and over **(f)** the South Pacific Ocean (site code: HPB) on 9 November 2009. The blue lines show the profiles of observation data, including aircraft measurements. The red lines show the GOSAT a priori profiles. The black lines are GOSAT CAKs. Aircraft-based XCO_2 without the application of GOSAT CAK and the differences between aircraft-based XCO_2 with and without the application of GOSAT CAK are indicated by blue and green letters, respectively.

when the difference between aircraft-based XCO_2 with and without the application of CAK was larger (0.132 ppm) over Narita during the analysis period. As is clear from Fig. 3a, the XCO_2 values of tower measurement were not coincident with those of GOSAT a priori. It was assumed that this disagreement (i.e., the shape of the a priori profile) was one reason for the increase in XCO_2 difference associated with the application of CAK. In the case of 6 April 2010, vertical profiles of the aircraft and tower agreed well with those of the a priori profile (Fig. 3b), and hence the difference between aircraft-based XCO_2 with and without CAK was as small as 0.046 ppm. Figure 3c shows an example of vertical profiles in Honolulu, Hawaii. As there is no meteorological tower, the concentration of the lowest observational altitude of an airliner has been extended down to the surface. The CO_2 concentration was lower in the upper troposphere and higher above the tropopause (Fig. 3c). This may be explained by meridional transport of CO_2 from the tropical troposphere in the northern summer (Sawa et al., 2008). In the Southern Great Plains (Oklahoma, USA), two examples for the northern summer and winter are given (Fig. 3d, e). The CO_2 concentration is clearly lower near the surface and higher in the midtroposphere in summer, whereas CO_2 densities in winter decrease with height. We also show an example of the HIPPO data in Fig. 3f.

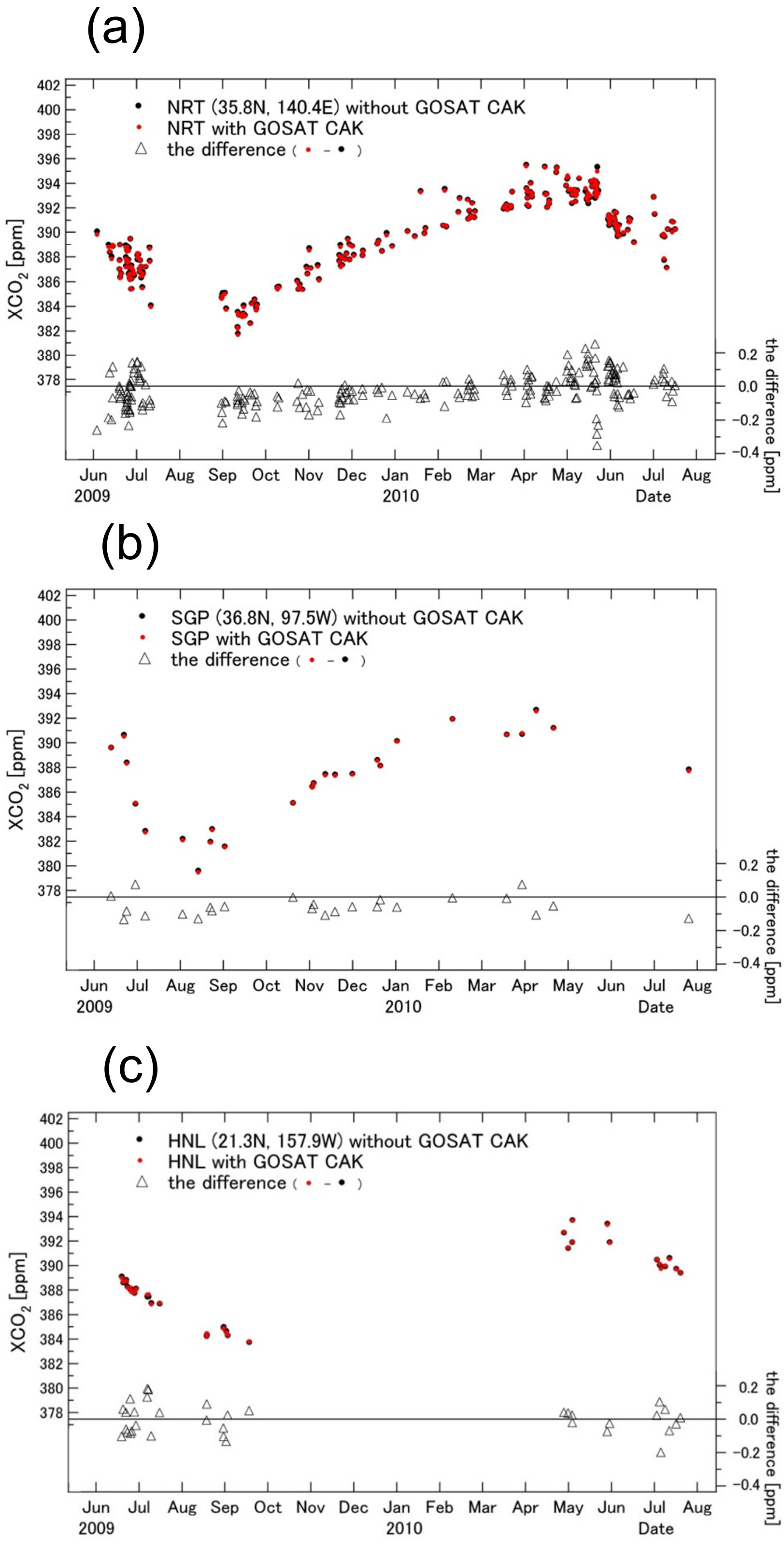

Fig. 4. Temporal variations of XCO$_2$ with and without CAK in **(a)** Narita, **(b)** the Southern Great Plains, and **(c)** Honolulu. Red and black closed circles indicate XCO$_2$ with and without the application of CAK, respectively. Open triangles denote the differences between XCO$_2$ with CAK and without CAK.

Figure 4a shows the temporal variations of aircraft-based XCO_2 over Narita (Northern Hemisphere) from June 2009 to July 2010. A total of 225 temporally matched cases were obtained. Both data with and without CAK showed that XCO_2 is higher in spring and lower from late summer through autumn. Open triangles denote the differences, which are less than ± 0.2 ppm in most cases. As listed in Table 2, the average of all differences between aircraft-based XCO_2 with and without the application of GOSAT CAK (aircraft-based XCO_2 with CAK minus aircraft-based XCO_2 without CAK) in Narita is as small as -0.030 ± 0.095 ppm, and it can be assumed that the GOSAT SWIR CAK has only a minor effect on the aircraft-based XCO_2 calculation over Narita. We also present temporal variations and the impacts of GOSAT CAK for the Southern Great Plains and Honolulu (Fig. 4b and c). Temporally matched data were confined to the period between late spring and early autumn in Honolulu (Fig. 4c). This may be attributed to sunglint observation, which is conducted by utilizing specular reflection over ocean regions where surface reflectance is small (e.g., Kuze et al., 2009). Consequently, 671 samples were extracted from 41 observation sites, and the average of all differences was -0.022 ppm with a standard deviation of 0.088 ppm (Table 2).

The differences between aircraft-based XCO_2 with CAK and without CAK were evaluated to be less than ±0.4 ppm at most, and less than ±0.1 ppm on average (Table 2). Therefore, we concluded that the GOSAT SWIR CAK had a minor effect on the aircraft-based XCO_2 calculation.

4.2 Impact of model profiles in the stratosphere and mesosphere on the aircraft-based XCO_2 calculation

In addition to ACTM, two more model outputs were used as the middle atmosphere profiles to investigate the impact. We calculated XCO_2 from aircraft profiles using ACTM, a priori profiles as in GOSAT retrieval (Maksyutov et al., 2008, see Sect. 3.1.4), and a priori profiles of TCCON (Wunch et al., 2010) as stratospheric and mesospheric profiles at four aircraft sites (Park Falls, the Southern Great Plains, Narita, and Sydney), located near the TCCON sites – Park Falls, Lamont (Oklahoma, USA), Tsukuba (Japan), and Wollongong (Australia). Column abundances calculated from the three model profiles were referred to as "ACTM XCO_2," "GOSAT prior XCO_2," and "TCCON prior XCO_2," respectively. Figure 5 shows an example for Narita on 28 November 2009, including profiles by ACTM, GOSAT a priori profile, and TCCON a priori profile. Here, the difference between "ACTM XCO_2" and "GOSAT prior XCO_2" was as small as 0.011 ppm, and the difference between "ACTM XCO_2" and "TCCON prior XCO_2" was -0.133 ppm. The averages obtained at the four respective observation sites are listed in Table 3. The average of "ACTM XCO_2 minus TCCON prior XCO_2" over Park Falls was -0.311 ± 0.076 ppm. This result was consistent with that of Saito et al. (2012), who showed that the XCO_2 difference between the ACTM and TCCON

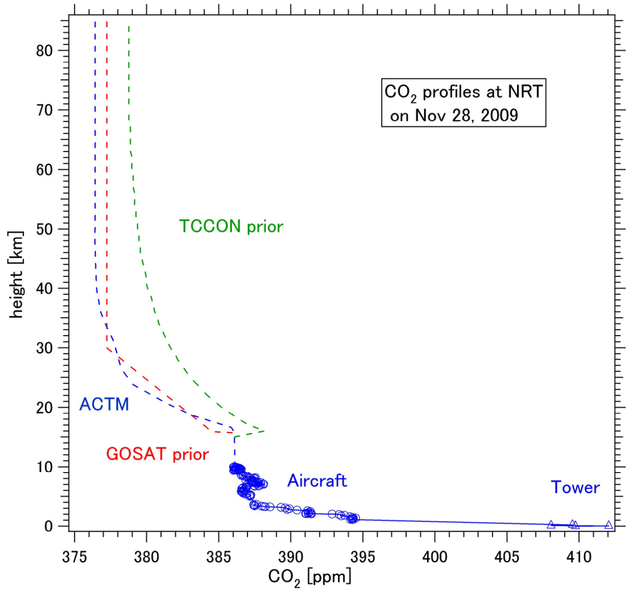

Fig. 5. Vertical profiles of CO_2 over Narita on 28 November 2009. Blue, red, and green dashed lines above the tropopause indicate profiles by ACTM, a priori as in the GOSAT retrieval, and a priori of TCCON, respectively. The blue solid lines show observation data, including aircraft measurements.

was -0.4 ppm (note that their results were based on profiles in all layers of the ACTM and TCCON). The results of 116 examples obtained at four observation sites indicated that the difference between "ACTM XCO_2" and "GOSAT prior XCO_2" was as small as 0.125 ± 0.334 ppm. On the other hand, "ACTM XCO_2 minus TCCON prior XCO_2" was -0.161 ± 0.098 ppm. Although the XCO_2 differences varied by region, the amount of CO_2 above the tropopause was small, and consequently did not have a large effect on the aircraft-based XCO_2 calculation at the four observation sites.

4.3 Comparison between GOSAT XCO_2 and aircraft-based XCO_2

We compared the GOSAT data observed within ±2 and ±5° latitude/longitude boxes centered at each observation site with aircraft-based data. Figure 6 shows comparisons between aircraft-based XCO_2 with the application of CAK and GOSAT data. In addition, the average and 1σ of the differences between GOSAT XCO_2 and aircraft-based XCO_2 at each site are listed in Table 4. For the ±2° boxes, there were a total of 74 observations over land and 11 over oceans, whereas there were a total of 182 observations over land and 40 over oceans for the ±5° boxes. In ocean regions, the mean biases of GOSAT data relative to aircraft measurements were -1.82 ppm with a standard deviation between two datasets of 1.04 and -2.27 ppm with a standard deviation of 1.79 ppm for the ±2 and ±5° boxes, respectively. Correlation coefficients between both datasets were 0.96 and 0.82

Table 2. The average, maximum, minimum, and 1 standard deviation (1σ) of the differences between aircraft-based XCO_2 with and without the application of GOSAT CAK (aircraft-based XCO_2 with CAK minus aircraft-based XCO_2 without CAK) at each aircraft observation site.

site	number	average [ppm]	1σ [ppm]	maximum [ppm]	minimum [ppm]
AMS	10	0.041	0.071	0.109	−0.100
LHR	5	−0.073	0.088	0.023	−0.204
YVR	7	0.005	0.085	0.115	−0.165
CDG	5	0.173	0.070	0.247	0.083
MXP	2	0.031	0.015	0.042	0.020
FCO	2	0.141	0.000	0.141	0.141
ICN	2	0.033	0.011	0.041	0.025
NRT	225	−0.030	0.095	0.245	−0.360
HND	17	0.052	0.084	0.188	−0.085
NGO	37	−0.056	0.077	0.127	−0.245
KIX	21	−0.069	0.091	0.090	−0.197
DEL	6	0.021	0.035	0.062	−0.026
TPE	1	−0.058	–	−0.058	−0.058
HNL	35	−0.008	0.088	0.174	−0.207
MNL	2	−0.019	0.109	0.058	−0.096
BKK	33	0.004	0.067	0.136	−0.133
GUM	0	–	–	–	–
SIN	13	−0.050	0.095	0.070	−0.249
CGK	10	−0.043	0.041	0.024	−0.114
SYD	52	−0.033	0.074	0.062	−0.229
PFA	0	–	–	–	–
BRM	1	−0.010	–	−0.010	−0.010
ESP	0	–	–	–	–
DND	7	0.039	0.060	0.140	−0.045
LEF	17	0.035	0.067	0.157	−0.132
NHA	17	0.007	0.108	0.252	−0.105
WBI	12	−0.037	0.055	0.084	−0.109
THD	3	0.009	0.035	0.041	−0.028
BNE	5	0.034	0.030	0.066	−0.011
CAR	20	−0.014	0.078	0.124	−0.223
HIL	17	−0.049	0.069	0.101	−0.135
AAO	29	0.002	0.074	0.122	−0.127
CMA	1	−0.039	–	−0.039	−0.039
SCA	9	−0.057	0.060	0.031	−0.157
TGC	7	−0.039	0.087	0.044	−0.210
RTA	5	−0.094	0.067	−0.017	−0.184
SGP	25	−0.065	0.057	0.067	−0.142
YAK	0	–	–	–	–
SUR	0	–	–	–	–
NOV	0	–	–	–	–
SGM	3	0.090	0.147	0.240	−0.055
HPA	1	−0.096	–	−0.096	−0.096
HPB	1	−0.099	–	−0.099	−0.099
HPC	1	−0.044	–	−0.044	−0.044
HPD	1	0.005	–	0.005	0.005
HPE	1	−0.166	–	−0.166	−0.166
TKB	3	−0.037	0.012	−0.023	−0.043
All data	671	−0.022	0.088	0.252	−0.360

Table 3. The average and 1 standard deviation (1σ) of the differences of aircraft-based XCO_2 calculated by using ACTM, a priori profiles of TCCON, and a priori profiles as in the GOSAT retrieval system in the stratosphere and mesosphere at each aircraft observation site.

		ACTM-TCCON prior		ACTM-GOSAT prior	
aircraft site (TCCON site)	number	average [ppm]	1σ [ppm]	average [ppm]	1σ [ppm]
LEF (Park Falls)	11	−0.311	0.076	−0.099	0.759
SGP (Lamont)	25	−0.176	0.083	0.461	0.337
NRT (Tsukuba)	60	−0.115	0.083	0.037	0.082
SYD (Wollongong)	20	−0.198	0.060	0.094	0.071
All data	116	−0.161	0.098	0.125	0.334

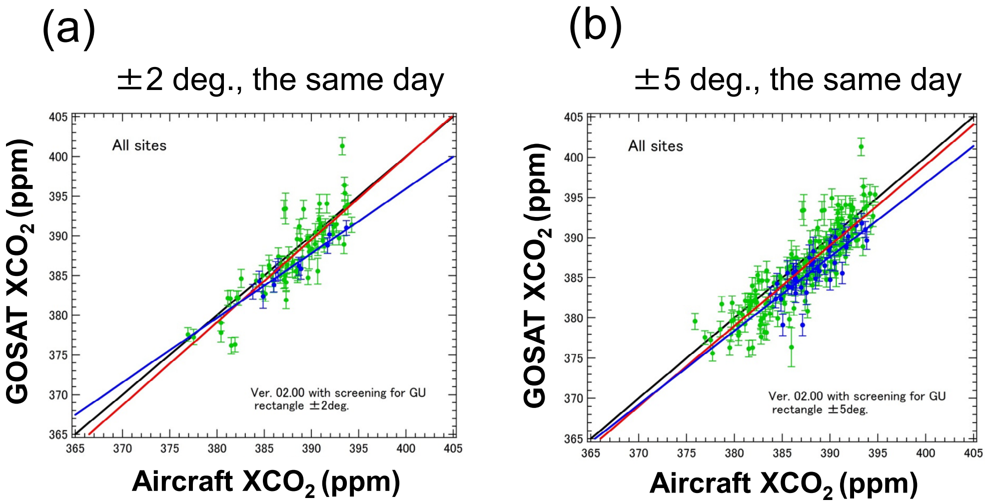

Fig. 6. Scatter diagrams between GOSAT XCO_2 observed within **(a)** ±2 and **(b)** ±5° latitude/longitude boxes centered at each aircraft observation site and aircraft-based XCO_2 with the application of CAK measured on a GOSAT overpass day. Green and blue dots indicate GOSAT XCO_2 obtained over land and ocean regions, respectively. Red and blue lines denote the regression lines with statistical significance at the 95 % level over land and ocean regions, respectively. The one-to-one lines are plotted as black lines.

with significance at the 99 % level, for XCO_2 data within the ±2 and ±5° boxes, respectively, though the sample size was small over ocean. Over the land regions, the mean biases of GOSAT SWIR XCO_2 relative to aircraft measurements were −0.68 ppm with a standard deviation between two datasets of 2.56 ppm, and −0.99 ppm with a standard deviation of 2.51 ppm, and the correlation coefficients were 0.85 and 0.86 with significance at the 99 % level for the ±2 and ±5° boxes, respectively. In general, the 1σ over land was larger than that over ocean regions. Aerosols and clouds are major sources of disturbance in GHG retrievals from space due to the modification of the equivalent optical path length (Mao and Kawa, 2004; Houweling et al., 2005; Reuter et al., 2010), and might produce a significant bias in the retrieved XCO_2 (Uchino et al., 2012). The atmosphere over ocean regions appears to be cleaner due to the absence of polluted air and aerosols from urban areas, whereas GOSAT XCO_2 retrieval in several land regions may be profoundly affected by polluted air and urban aerosols.

Finally, the validation results by the direct comparison were compared with those by the curve fitting method shown in the Supplement. Table 5 summarizes the average and 1σ of the differences between GOSAT XCO_2 and aircraft-based XCO_2 for all sites by direct comparison and the curve fitting method. The 1σ over land by the curve fitting method (2.36 and 2.37 ppm for ±2 and ±5° boxes, respectively) was smaller than that by the direct comparisons (2.56 and 2.51 ppm for ±2 and ±5° boxes, respectively). This implies that the curve fitting method could remove some errors by fitting the aircraft-based XCO_2 despite adding uncertainties due to the curve fitting. On the other hand, the overall bias over land by the curve fitting (−1.6 and −1.8 ppm for ±2 and ±5° boxes, respectively) was larger than that by the direct comparisons (−0.7 and −1.0 ppm for ±2 and ±5° boxes, respectively). The mean bias over land by the curve fitting method was consistent with that of Yoshida et al. (2013), who compared the GOSAT data with the TCCON data (−1.48 ppm). Also, 1σ of the GOSAT bias over land calculated using aircraft measurements (2.56 and 2.36 ppm

Table 4. The average and 1 standard deviation (1σ) of the differences between GOSAT XCO_2 and aircraft-based XCO_2 at each site. The GOSAT data were retrieved over (a) land and (b) ocean regions within ±2 and ±5° latitude/longitude boxes centered at each aircraft observation site.

(a) Land site	number	±2 deg. average [ppm]	1σ [ppm]	number	±5 deg. average [ppm]	1σ [ppm]
NRT	25	−0.212	2.646	40	−0.266	2.448
LHR	0	–	1.733	3	−3.173	1.733
YVR	0	–	2.232	6	−1.039	2.232
MXP	0	–	1.943	2	−0.182	1.943
ICN	1	0.331	–	1	0.331	–
NGO	6	0.093	3.732	11	0.366	2.817
KIX	1	−1.076	–	4	−1.299	2.781
TPE	0	–	–	1	4.705	–
BKK	0	–	–	4	−3.832	4.028
SYD	2	−0.630	1.172	9	−1.863	1.922
DND	0	–	–	1	−0.779	–
LEF	1	−2.621	–	5	−2.886	1.963
NHA	1	−1.705	–	7	0.061	1.852
WBI	1	−5.608	–	10	−1.417	2.301
THD	1	−1.978	–	1	−1.978	–
BNE	0	–	–	2	−3.198	0.754
CAR	1	−2.601	–	9	−2.500	2.667
HIL	7	−1.369	1.752	11	−1.465	1.644
AAO	6	−0.488	1.362	20	−0.331	2.267
SCA	6	−0.919	2.320	7	−0.090	1.192
TGC	1	2.470	–	5	−0.924	2.517
SGP	9	−2.662	1.677	16	−2.656	1.876
SGM	2	3.630	3.739	2	3.630	3.739
HPA	0	–	–	1	−3.471	–
HPE	0	–	–	1	−2.158	–
TKB	3	1.118	1.874	3	1.118	1.874
All data	74	−0.678	2.559	182	−0.991	2.506

(b) Ocean site	number	±2 deg. average [ppm]	1σ [ppm]	number	±5 deg. average [ppm]	1σ [ppm]
NRT	0	–	–	3	−4.549	3.880
FCO	0	–	–	1	0.043	–
NGO	0	–	–	3	−2.212	1.875
KIX	0	–	–	2	−3.766	3.073
HNL	6	−1.749	1.022	14	−1.679	0.976
BKK	1	−2.924	–	2	−3.562	0.902
SIN	0	–	–	2	−2.222	1.066
CGK	1	−0.701	–	1	−0.701	–
SYD	0	–	–	3	−1.683	1.617
NHA	0	–	–	1	−5.697	–
SCA	0	–	–	2	−2.483	1.601
RTA	1	−0.654	–	3	−1.875	1.327
HPB	0	–	–	1	−0.563	–
HPC	1	−2.232	–	1	−2.232	–
HPD	1	−3.061	–	1	−3.061	–
All data	11	−1.824	1.039	40	−2.269	1.792

Table 5. The average and 1 standard deviation (1σ) of the differences between GOSAT XCO_2 and aircraft-based XCO_2 for all sites by direct comparison and the curve fitting method.

±2 deg.	direct comparison			curve fitting method		
	number	average [ppm]	1σ [ppm]	number	average [ppm]	1σ [ppm]
Land	74	−0.68	2.56	2313	−1.56	2.36
Ocean	11	−1.82	1.04	85	−1.52	2.02
±5 deg.	direct comparison			curve fitting method		
	number	average [ppm]	1σ [ppm]	number	average [ppm]	1σ [ppm]
Land	182	−0.99	2.51	11146	−1.81	2.37
Ocean	40	−2.27	1.79	708	−1.73	2.35

for the direct comparison and the curve fitting method within ±2° boxes, respectively) was larger than that calculated using TCCON data (2.09 ppm). This difference may be partly attributed to the fact that TCCON data were used as time-averaged data (e.g., averages of the data obtained within ±30 min of the GOSAT overpass time) for comparing to the GOSAT XCO_2, whereas aircraft measurement data were momentarily obtained at respective heights.

We suggest that the present version (ver. 02.00) of GOSAT FTS-SWIR XCO_2 products is a significant improvement on the previous version (ver. 01.xx), which produced values approximately 9 ppm lower than ground-based FTS data in several locations across the globe (Morino et al., 2011). In addition, our results with aircraft measurements were similar to those of Yoshida et al. (2013), who validated GOSAT XCO_2 with the TCCON data. The GOSAT XCO_2 data (ver. 02.00) observed over not only land but also ocean regions are significantly correlated with aircraft measurement data.

5 Summary and conclusions

This paper presents a validation of XCO_2 derived from GOSAT TANSO-FTS SWIR (ver. 02.00) using aircraft measurement data obtained from CONTRAIL, NOAA, DOE, NIES, the HIPPO program, and the NIES-JAXA campaign. Prior to the GOSAT validation, we examined how the aircraft-based XCO_2 changes following application of the GOSAT SWIR CAK. The differences between aircraft-based XCO_2 with and without CAK were evaluated to be less than ±0.4 ppm at most, and less than ±0.1 ppm on average. Therefore, we concluded that the GOSAT CAK had only a minor effect on the aircraft-based XCO_2 calculation.

We performed a comparison between GOSAT SWIR XCO_2 observed within ±2 or ±5° latitude/longitude boxes at each site and aircraft-based XCO_2 measured on a GOSAT overpass day. These results indicated that GOSAT XCO_2 over land regions agreed with aircraft-based XCO_2, except that the former is biased by −0.68 ppm (−0.99 ppm) with a standard deviation of 2.56 ppm (2.51 ppm), whereas the averages of the differences between the GOSAT XCO_2 over ocean and the aircraft-based XCO_2 were −1.82 ppm (−2.27 ppm) with a standard deviation of 1.04 ppm (1.79 ppm) for ±2° (±5°) boxes. The curve fitting method would be also useful as an alternative validation method. Finally, the present version (ver. 02.00) of GOSAT SWIR products was a significant improvement on the earlier version (ver. 01.xx), which produced values approximately 9 ppm lower than reference data (Morino et al., 2011). However, the standard deviations of the differences between GOSAT XCO_2 and aircraft-based XCO_2 were not as small, being around 3 ppm at several sites. Further studies are required to investigate the causes of this finding with a focus on the correlation between GOSAT SWIR XCO_2 and several simultaneously retrieved variables, including aerosol optical depth and surface albedo.

Supplementary material related to this article is available online at http://www.atmos-chem-phys.net/13/9771/2013/acp-13-9771-2013-supplement.pdf.

Acknowledgements. The authors thank the many staff members of Japan Airlines, the JAL Foundation, and JAMCO Tokyo for supporting the CONTRAIL project. We are grateful to the NOAA ESRL/GMD tall tower network (K. Davis, A. Desai, R. Teclaw, D. Baumann, and C. Stanier) for providing LEF and WBI CO_2 tower data. DOE flights were supported by the Office of Biological and Environmental Research of the US Department of Energy under contract No. DE-AC02-05CH11231 as part of the Atmospheric Radiation Measurement Program (ARM), ARM Aerial Facility, and Terrestrial Ecosystem Science Program. We also thank the HIPPO team members for CO_2 profile data by HIPPO missions and Steven C. Wofsy at Harvard University for his useful suggestions. The HIPPO program is supported by the National Science Foundation (NSF), and its operations are managed by the Earth Observing Laboratory (EOL) of the National Center for Atmospheric Research (NCAR). TCCON a priori profiles were obtained from the TCCON data archive, operated by the

California Institute of Technology (http://tccon.ipac.caltech.edu/). US support for TCCON retrieval software and the development of these data comes from NASA's Carbon Cycle Science Program and NASA's OCO-2 project. This research was supported in part by the Environment Research and Technology Development Fund (2A-1102) of the Ministry of the Environment, Japan.

Edited by: M. K. Dubey

References

Andrews, A. E., Kofler, J., Bakwin, P. S., Zhao, C., and Tans, P.: Carbon dioxide and carbon monoxide dry air mole fractions from the NOAA ESRL tall tower network, 1992-2009, Version: 2011-08-31, available at: ftp://ftp.cmdl.noaa.gov/ccg/towers/ (last access: July 2013), 2011.

Araki, M., Morino, I., Machida, T., Sawa, Y., Matsueda, H., Ohyama, H, Yokota, T., and Uchino, O.: CO_2 column-averaged volume mixing ratio derived over Tsukuba from measurements by commercial airlines, Atmos. Chem. Phys., 10, 7659–7667, doi:10.5194/acp-10-7659-2010, 2010.

Biraud, S. C., Torn, M. S., Smith, J. R., Sweeney, C., Riley, W. J., and Tans, P. P.: A multi-year record of airborne CO_2 observations in the US Southern Great Plains, Atmos. Meas. Tech., 6, 751–763, doi:10.5194/amt-6-751-2013, 2013.

Chédin, A., Serrar, S., Armante, R., and Scott, N. A.: Signatures of annual and seasonal variations of CO_2 and other greenhouse gases from comparisons between NOAA TOVS observations and radiation model simulations, J. Climate, 15, 95–116, 2002.

Christi, M. J. and Stephens, G. L.: Retrieving profiles of atmospheric CO_2 in clear sky and in the presence of thin cloud using spectroscopy from the near and thermal infrared: a preliminary case study. J. Geophys. Res., 109, D04316, doi:10.1029/2003JD004058, 2004.

Connor, B. J., Bösch, H., Toon, G., Sen, B., Miller, C., and Crisp, D.: Orbiting carbon observatory: inverse method and prospective error analysis, J. Geophys. Res., 113, D05305, doi:10.1029/2006JD008336, 2008.

Conway, T. J., Tans, P., Waterman, L. S., Thoning, K. W., Masarie, K. A., and Gammon, R. H.: Atmospheric carbon dioxide measurements in the remote global troposphere, 1981–1984, Tellus B, 40, 81–115, 1988.

Crevoisier, C., Heilliette, S., Chédin, A., Serrar, S., Armante, R., and Scott, N. A.: Midtropospheric CO_2 concentration retrieval from AIRS observations in the tropics. Geophys. Res. Lett., 31, L17106, doi:10.1029/2004GL020141, 2004.

Dils, B., De Mazière, M., Müller, J. F., Blumenstock, T., Buchwitz, M., de Beek, R., Demoulin, P., Duchatelet, P., Fast, H., Frankenberg, C., Gloudemans, A., Griffith, D., Jones, N., Kerzenmacher, T., Kramer, I., Mahieu, E., Mellqvist, J., Mittermeier, R. L., Notholt, J., Rinsland, C. P., Schrijver, H., Smale, D., Strandberg, A., Straume, A. G., Stremme, W., Strong, K., Sussmann, R., Taylor, J., van den Broek, M., Velazco, V., Wagner, T., Warneke, T., Wiacek, A., and Wood, S.: Comparisons between SCIAMACHY and ground-based FTIR data for total columns of CO, CH_4, CO_2 and N_2O, Atmos. Chem. Phys., 6, 1953–1976, doi:10.5194/acp-6-1953-2006, 2006.

Enting, I. G.: Inverse problems in atmospheric constituent transport. Cambridge University Press, Cambridge, UK, 393 pp., 2002.

Fleming, E. L., Chandra, S., Barnett, J. J., and Corney, M.: Zonal mean temperature, pressure, zonal wind and geopotential height as functions of latitude, COSPAR international reference atmosphere: 1986, Part II: middle atmosphere models, Adv. Space Res., 10, 11–59, doi:10.1016/0273-1177(90)90386-E, 1990.

Gurney, K. R., Law, R. M., Denning, A. S., Rayner, P. J., Baker, D., Bousquet, P., Bruhwiler, L., Chen, Y.-H., Ciais, P., Fan, S., Fung, I. Y., Gloor, M., Heimann, M., Higuchi, K., John, J., Maki, T., Maksyutov, S., Masarie, K., Peylin, P., Prather, M., Pak, B. C., Randerson, J., Sarmiento, J., Taguchi, S., Takahashi, T., and Yuen, C.-W.: Towards robust regional estimates of CO_2 sources and sinks using atmospheric transport models, Nature, 415, 626–630, doi:10.1038/415626a, 2002.

Heymann, J., Bovensmann, H., Buchwitz, M., Burrows, J. P., Deutscher, N. M., Notholt, J., Rettinger, M., Reuter, M., Schneising, O., Sussmann, R., and Warneke, T.: SCIAMACHY WFM-DOAS XCO_2: reduction of scattering related errors, Atmos. Meas. Tech., 5, 2375–2390, doi:10.5194/amt-5-2375-2012, 2012.

Houweling, S., Hartmann, W., Aben, I., Schrijver, H., Skidmore, J., Roelofs, G.-J., and Breon, F.-M.: Evidence of systematic errors in SCIAMACHY-observed CO_2 due to aerosols, Atmos. Chem. Phys., 5, 3003–3013, doi:10.5194/acp-5-3003-2005, 2005.

Inoue, H. Y. and Matsueda, H.: Variations in atmospheric CO_2 at the Meteorological Research Institute, Tsukuba, Japan, J. Atmos. Chem., 23, 137–161, 1996.

Inoue, H. Y. and Matsueda, H.: Measurements of atmospheric CO_2 from a meteorological tower in Tsukuba, Japan, Tellus B, 53, 205–219, doi:10.1034/j.1600-0889.2001.01163.x, 2001.

Kida, H.: General circulation of air parcels and transport characteristics derived from a hemispheric GCM, part 2, very long-term motions of air parcels in the troposphere and stratosphere, J. Meteor. Soc. Jpn., 61, 510–522, 1983.

Komhyr, W. D., Harris, T. B., Waterman, L. S., Chin, J. F. S., and Thoning, K. W.: Atmospheric carbon dioxide at Mauna Loa Observatory 1. NOAA global monitoring for climatic change measurements with a nondispersive infrared analyzer, 1974–1985, J. Geophys. Res., 94, 8533–8547, doi:10.1029/JD094iD06p08533, 1989.

Kuze, A., Suto, H., Nakajima, M., and Hamazaki, T.: Thermal and near infrared sensor for carbon observation Fourier-transform spectrometer on the Greenhouse Gases Observing Satellite for greenhouse gases monitoring, Appl. Optics, 48, 6716–6733, doi:10.1364/AO.48.006716, 2009.

Machida, T., Nakazawa, T., Ishidoya, S., Maksyutov, S., Tohjima, Y., Takahashi, Y., Watai, T., Vinnichenko, N., Panchenko, M., Arshinov, M., Fedoseev, N., and Inoue, G: Temporal and spatial variations of atmospheric CO_2 mixing ratio over Siberia, Ext. Abstr., in: 6th International CO_2 Conf., 1–5 October, Sendai, Japan, 2001.

Machida, T., Matsueda, H., Sawa, Y., Nakagawa, Y., Hirotani, K., Kondo, N., Goto, K., Nakazawa, T., Ishikawa, K., and Ogawa, T.: Worldwide measurements of atmospheric CO_2 and other trace gas species using commercial airlines, J. Atmos. Ocean. Technol., 25, 1744–1754, doi:10.1175/2008JTECHA1082.1, 2008.

Maddy, E. S., Barnet, C. D., Goldberg, M., Sweeney, C., and Liu, X.: CO_2 retrievals from the Atmospheric Infrared Sounder: Methodology and validation, J. Geophys. Res., 113, D11301, doi:10.1029/2007JD009402, 2008.

Maksyutov, S., Patra, P. K., Onishi, R., Saeki, T., and Nakazawa, T.: NIES/FRCGC global atmospheric tracer transport model: Description, validation, and surface sources and sinks inversion, J. Earth Sim., 9, 3–18, 2008.

Maksyutov, S., Takagi, H., Valsala, V. K., Saito, M., Oda, T., Saeki, T., Belikov, D. A., Saito, R., Ito, A., Yoshida, Y., Morino, I., Uchino, O., Andres, R. J., and Yokota, T.: Regional CO_2 flux estimates for 2009–2010 based on GOSAT and ground-based CO_2 observations, Atmos. Chem. Phys., 13, 9351–9373, doi:10.5194/acp-13-9351-2013, 2013.

Mao, J. and Kawa, S. R.: Sensitivity studies for space-based measurement of atmospheric total column carbon dioxide by reflected sunlight, Appl. Optics, 43, 914-927, 2004.

Matsueda, H., Inoue, H. Y., and Ishii, M.: Aircraft observation of carbon dioxide at 8–13 km altitude over the Western Pacific from 1993 to 1999, Tellus B, 54, 1–21, 2002.

Matsueda, H., Machida, T., Sawa, Y., Nakagawa, Y., Hirotani, K., Ikeda, H., Kondo, N., and Goto, K.: Evaluation of atmospheric CO_2 measurements from new flask air sampling of JAL airliner observations, Pap. Meteorol. Geophys., 59, 1–17, 2008.

Messerschmidt, J., Geibel, M. C., Blumenstock, T., Chen, H., Deutscher, N. M., Engel, A., Feist, D. G., Gerbig, C., Gisi, M., Hase, F., Katrynski, K., Kolle, O., Lavrič, J. V., Notholt, J., Palm, M., Ramonet, M., Rettinger, M., Schmidt, M., Sussmann, R., Toon, G. C., Truong, F., Warneke, T., Wennberg, P. O., Wunch, D., and Xueref-Remy, I.: Calibration of TCCON column-averaged CO_2: the first aircraft campaign over European TCCON sites, Atmos. Chem. Phys., 11, 10765–10777, doi:10.5194/acp-11-10765-2011, 2011.

Messerschmidt, J., Chen, H., Deutscher, N. M., Gerbig, C., Grupe, P., Katrynski, K., Koch, F.-T., Lavrič, J. V., Notholt, J., Rödenbeck, C., Ruhe, W., Warneke, T., and Weinzierl, C.: Automated ground-based remote sensing measurements of greenhouse gases at the Białystok site in comparison with collocated in situ measurements and model data, Atmos. Chem. Phys., 12, 6741–6755, doi:10.5194/acp-12-6741-2012, 2012.

Miyamoto, Y., Inoue, M., Morino, I., Uchino, O., Yokota, T., Machida, T., Sawa, Y., Matsueda, H., Sweeney, C., Tans, P. P., Andrews, A. E., Biraud, S. C., and Patra, P. K.: Atmospheric column-averaged mole fractions of carbon dioxide at 53 aircraft measurement sites, Atmos. Chem. Phys., 13, 5265–5275, doi:10.5194/acp-13-5265-2013, 2013.

Morino, I., Uchino, O., Inoue, M., Yoshida, Y., Yokota, T., Wennberg, P. O., Toon, G. C., Wunch, D., Roehl, C. M., Notholt, J., Warneke, T., Messerschmidt, J., Griffith D. W. T., Deutscher, N. M., Sherlock, V., Connor, B., Robinson, J., Sussmann, R., and Rettinger, M.: Preliminary validation of column-averaged volume mixing ratios of carbon dioxide and methane retrieved from GOSAT short-wavelength infrared spectra, Atmos. Meas. Tech., 4, 1061– 1076, doi:10.5194/amt-4-1061-2011, 2011.

Nakakita, E., Ikebuchi, S., Nakamura, T., Kanmuri, M., Okuda, M., Yamaji, A., and Takasao, T.: Short-term rainfall prediction method using a volume scanning radar and grid point value data from numerical weather prediction, J. Geophys. Res., 101, 26181–26197, 1996.

Nakazawa, T., Machida, T., Sugawara, S., Murayama, S., Morimoto, S., Hashida, G., Honda, H., and Itoh, T.: Measurements of the stratospheric carbon dioxide concentration over Japan using a balloon-borne cryogenic sampler, Geophys. Res. Lett., 22, 1229–1232, doi:10.1029/95GL01188, 1995.

Nakazawa, T., Ishizawa, M., Higuchi, K., and Trivett, N. B. A.: Two curve fitting methods applied to CO_2 flask data, Environmetrics, 8, 197–218, 1997a.

Nakazawa, T., Morimoto, S., Aoki, S., and Tanaka, M.: Temporal and spatial variations of the carbon isotopic ratio of atmospheric carbon dioxide in the western Pacific region, J. Geophys. Res., 102, 1271–1285, 1997b.

Nakazawa, T., Sugawara, S., Inoue, G., Machida, T., Maksyutov, S., and Mukai, H.: Aircraft measurements of the concentrations of CO_2, CH_4, N_2O, and CO and the carbon and oxygen isotopic ratios of CO_2 in the troposphere over Russia, J. Geophys. Res., 102, 3843–3859, 1997c.

Niwa, Y., Machida, T., Sawa, Y., Matsueda, H., Schuck, T. J., Brenninkmeijer, C. A. M., Imasu, R., and Satoh, M.: Imposing strong constraints on tropical terrestrial CO_2 fluxes using passenger aircraft based measurements, J. Geophys. Res., 117, D11303, doi:10.1029/2012JD017474, 2012.

NOAA/ESRL Carbon Cycle Greenhouse Gases Aircraft Program, available at: http://www.esrl.noaa.gov/gmd/ccgg/aircraft/index.html (last access: July 2013), 2012.

Numaguti, A., Takahashi, M., Nakajima, T., and Sumi, A.: Development of CCSR/NIES atmospheric general circulation model, in: Reports of a New Program for Creative Basic Research Studies, CGER's Supercomputer. Monogr. Rep., 3, CGER, National Institute for Environmental Studies, Tsukuba, Japan, 1–48, 1997.

Ohyama, H., Morino, I., Nagahama, T., Machida, T., Suto, H., Oguma, H., Sawa, Y., Matsueda, H., Sugimoto, N., Nakane, H., and Nakagawa, K.: Column-averaged volume mixing ratio of CO_2 measured with ground-based Fourier transform spectrometer at Tsukuba, J. Geophys. Res., 114, D18303, doi:10.1029/2008JD011465, 2009.

Oshchepkov, S., Bril, A., Yokota, T., Wennberg, P. O., Deutscher, N. M., Wunch, D., Toon, G. C., Yoshida, Y., O'Dell, C. W., Crisp, D., Miller, C. E., Frankenberg, C., Butz, A., Aben, I., Guerlet, S., Hasekamp, O., Boesch, H., Cogan, A., Parker, R., Griffith, D., Macatangay, R., Notholt, J., Sussmann, R., Rettinger, M., Sherlock, V., Robinson, J., Kyrö, E., Heikkinen, P., Feist, D. G., Morino, I., Kadygrov, N., Belikov, D., Maksyutov, S., Matsunaga, T., Uchino, O., and Watanabe, H.: Effects of atmospheric light scattering on spectroscopic observations of greenhouse gases from space. Part 2: Algorithm intercomparison in the GOSAT data processing for CO_2 retrievals over TCCON sites, J. Geophys. Res., 118, 1493–1512, doi:10.1002/jgrd.50146, 2013.

Pales, J. C. and Keeling, C. D.: The concentration of atmospheric carbon dioxide in Hawaii, J. Geophys. Res., 70, 6053–6076, doi:10.1029/JZ070i024p06053, 1965.

Pan, L. L. and Munchak, L. A.: Relationship of cloud top to the tropopause and jet structure from CALIPSO data, J. Geophys. Res., 116, D12201, doi:10.1029/2010JD015462, 2011.

Patra, P. K., Takigawa, M., Dutton, G. S., Uhse, K., Ishijima, K., Lintner, B. R., Miyazaki, K., and Elkins, J. W.: Transport mechanisms for synoptic, seasonal and interannual SF_6 variations and "age" of air in troposphere, Atmos. Chem. Phys., 9, 1209–1225, doi:10.5194/acp-9-1209-2009, 2009.

Patra, P. K., Niwa, Y., Schuck, T. J., Brenninkmeijer, C. A. M., Machida, T., Matsueda, H., and Sawa Y.: Carbon balance of South Asia constrained by passenger aircraft

CO_2 measurements, Atmos. Chem. Phys., 11, 4163–4175, doi:10.5194/acp-11-4163-2011, 2011.

Rayner, P. J. and O'Brien, D. M.: The utility of remotely sensed CO_2 concentration data in surface source inversions, Geophys. Res. Lett., 28, 175–178, 2001.

Reuter, M., Buchwitz, M., Schneising, O., Heymann, J., Bovensmann, H., and Burrows, J. P.: A method for improved SCIAMACHY CO_2 retrieval in the presence of optically thin clouds, Atmos. Meas. Tech., 3, 209–232, doi:10.5194/amt-3-209-2010, 2010.

Rodgers, C. D. and Connor, B. J.: Intercomparison of remote sounding instruments, J. Geophys. Res., 108, 4116, doi:10.1029/2002JD002299, 2003.

Saeki, T., Maksyutov, S., Saito, M., Valsala, V., Oda, T., Andres, R. J., Belikov, D., Tans, P., Dlugokencky, E., Yoshida, Y., Morino, I., Uchino, O., and Yokota, T.: Inverse modeling of CO_2 fluxes using GOSAT data and multi-year ground-based observations, Sci. Online Lett. Atmos. (SOLA), 9, 45–50, doi:10.2151/sola.2013-011, 2013.

Saito, R., Patra, P. K., Deutscher, N., Wunch, D., Ishijima, K., Sherlock, V., Blumenstock, T., Dohe, S., Griffith, D., Hase, F., Heikkinen, P., Kyrö, E., Macatangay, R., Mendonca, J., Messerschmidt, J., Morino, I., Notholt, J., Rettinger, M., Strong, K., Sussmann, R., and Warneke, T.: Technical Note: Latitude-time variations of atmospheric column-average dry air mole fractions of CO_2, CH_4 and N_2O, Atmos. Chem. Phys., 12, 7767–7777, doi:10.5194/acp-12-7767-2012, 2012.

Saitoh, N., Imasu, R., Ota, Y., and Niwa, Y.: CO_2 retrieval algorithm for the thermal infrared spectra of the Greenhouse Gases Observing Satellite: potential of retrieving CO_2 vertical profile from high-resolution FTS sensor, J. Geophys. Res., 114, D17305, doi:10.1029/2008JD011500, 2009.

Sawa, Y., Machida, T., and Matsueda, H.: Seasonal variations of CO_2 near the tropopause observed by commercial aircraft, J. Geophys. Res., 113, D23301, doi:10.1029/2008JD010568, 2008.

Schneising, O., Bergamaschi, P., Bovensmann, H., Buchwitz, M., Burrows, J. P., Deutscher, N. M., Griffith, D. W. T., Heymann, J., Macatangay, R., Messerschmidt, J., Notholt, J., Rettinger, M., Reuter, M., Sussmann, R., Velazco, V. A., Warneke, T., Wennberg, P. O., and Wunch, D.: Atmospheric greenhouse gases retrieved from SCIAMACHY: comparison to ground-based FTS measurements and model results, Atmos. Chem. Phys., 12, 1527–1540, doi:10.5194/acp-12-1527-2012, 2012.

Takagi, H., Saeki, T., Oda, T., Saito, M., Valsala, V., Belikov, D., Saito, R., Yoshida, Y., Morino, I., Uchino, O., Andres, R. J., Yokota T., and Maksyutov, S.: On the Benefit of GOSAT Observations to the Estimation of Regional CO_2 Fluxes, Sci. Online Lett. Atmos. (SOLA), 7, 161–164, doi:10.2151/sola.2011-041, 2011.

Tanaka, T., Miyamoto, Y., Morino, I., Machida, T., Nagahama, T., Sawa, Y., Matsueda, H., Wunch, D., Kawakami, S., and Uchino, O.: Aircraft measurements of carbon dioxide and methane for the calibration of ground-based high-resolution Fourier Transform Spectrometers and a comparison to GOSAT data measured over Tsukuba and Moshiri, Atmos. Meas. Tech., 5, 2003–2012, doi:10.5194/amt-5-2003-2012, 2012.

Tans, P. P., Conway, T., and Nakazawa, T.: Latitudinal distribution of the sources and sinks of atmospheric carbon dioxide derived from surface observations and an Atmospheric Transport Model, J. Geophys. Res., 94, 5151–5172, 1989.

Uchino, O., Kikuchi, N., Sakai, T., Morino, I., Yoshida, Y., Nagai, T., Shimizu, A., Shibata, T., Yamazaki, A., Uchiyama, A., Kikuchi, N., Oshchepkov, S., Bril, A., and Yokota, T.: Influence of aerosols and thin cirrus clouds on the GOSAT-observed CO_2: a case study over Tsukuba, Atmos. Chem. Phys., 12, 3393–3404, doi:10.5194/acp-12-3393-2012, 2012.

Watanabe, F., Uchino, O., Joo, Y., Aono, M., Higashijima, K., Hirano, Y., Tsuboi, K., and Suda, K.: Interannual variation of growth rate of atmospheric carbon dioxide concentration observed at the JMA's three monitoring stations, J. Meteor. Soc. Jpn., 78, 673–682, 2000.

WMO: WMO Greenhouse Gas Bulletin, The State of Greenhouse Gases in the Atmosphere Using Global Observations through 2006, No. 3, World Meteorological Organization, 2007, available at: http://www.wmo.int/pages/prog/arep/gaw/ghg/ghgbull06_en.html (last access: July 2013), 2012.

WMO: WMO Greenhouse Gas Bulletin, The State of Greenhouse Gases in the Atmosphere Based on Global Observations through 2009, No. 6, World Meteorological Organization, 2010, available at: http://www.wmo.int/pages/prog/arep/gaw/ghg/ghgbull06_en.html (last access: July 2013), 2012.

Wofsy, S. C. and the HIPPO Science Team and Cooperating Modellers and Satellite Teams: HIAPER Pole-to-Pole Observations (HIPPO): fine-grained, global-scale measurements of climatically important atmospheric gases and aerosols, Philos. T. Roy. Soc. A, 369, 2073–2086, doi:10.1098/rsta.2010.0313, 2011.

Wofsy, S. C., Daube, B. C., Jimenez, R., Kort, E., Pittman, J. V., Park, S., Commane, R., Xiang, B., Santoni, G., Jacob, D., Fisher, J., Pickett-Heaps, C., Wang, H., Wecht, K., Wang, Q.-Q., Stephens, B. B., Shertz, S., Watt, A. S., Romashkin, P., Campos, T., Haggerty, J., Cooper, W. A., Rogers, D., Beaton, S., Hendershot, R., Elkins, J. W., Fahey, D. W., Gao, R. S., Moore, F., Montzka, S. A., Schwarz, J. P., Perring, A. E., Hurst, D., Miller, B. R., Sweeney, C., Oltmans, S., Nance, D., Hintsa, E., Dutton, G., Watts, L. A., Spackman, J. R., Rosenlof, K. H., Ray, E. A., Hall, B., Zondlo, M. A., Diao, M., Keeling, R., Bent, J., Atlas, E. L., Lueb, R., and Mahoney, M. J.: HIPPO Merged 10-second Meteorology, Atmospheric Chemistry, Aerosol Data (R_20121129), used data file "HIPPO_all_missions_merge_10s_20121129.tbl", Carbon Dioxide Information Analysis Center, Oak Ridge National Laboratory, Oak Ridge, Tennessee, USA, doi:10.3334/CDIAC/hippo_010 , 2012.

Wunch, D., Toon, G. C., Wennberg, P. O., Wofsy, S. C., Stephens, B. B., Fischer, M. L., Uchino, O., Abshire, J. B., Bernath, P., Biraud, S. C., Blavier, J.-F. L., Boone, C., Bowman, K. P., Browell, E. V., Campos, T., Connor, B. J., Daube, B. C., Deutscher, N. M., Diao, M., Elkins, J. W., Gerbig, C., Gottlieb, E., Griffith, D. W. T., Hurst, D. F., Jiménez, R., Keppel-Aleks, G., Kort, E. A., Macatangay, R., Machida, T., Matsueda, H., Moore, F., Morino, I., Park, S., Robinson, J., Roehl, C. M., Sawa, Y., Sherlock, V., Sweeney, C., Tanaka, T., and Zondlo, M. A.: Calibration of the Total Carbon Column Observing Network using aircraft profile data, Atmos. Meas. Tech., 3, 1351–1362, doi:10.5194/amt-3-1351-2010, 2010.

Wunch, D., Toon, G. C., Blavier, J.-F. L., Washenfelder, R. A., Notholt, J., Connor, B. J., Griffith, D. W. T., Sherlock, V., and Wennberg, P. O.: The Total Carbon Column Observing Network, Philos. T. Roy. Soc. A, 369, 2087–2112, doi:10.1098/rsta.2010.0240, 2011.

Yokota, T., Yoshida, Y., Eguchi, N., Ota, Y., Tanaka, T., Watanabe, H., and Maksyutov, S.: Global concentrations of CO_2 and CH_4 retrieved from GOSAT: first preliminary results, Sci. Online Lett. Atmos. (SOLA), 5, 160–163, doi:10.2151/sola.2009-041, 2009.

Yoshida, Y., Oguma, H., Morino, I., Suto, H., Kuze, A., and Yokota, T.: Mountaintop observation of CO_2 absorption spectra using a short wavelength infrared Fourier transform spectrometer, Appl. Optics, 49, 71–79, 2010.

Yoshida, Y., Ota, Y., Eguchi, N., Kikuchi, N., Nobuta, K., Tran, H., Morino, I., and Yokota, T.: Retrieval algorithm for CO_2 and CH_4 column abundances from short-wavelength infrared spectral observations by the Greenhouse gases observing satellite, Atmos. Meas. Tech., 4, 717–734, doi:10.5194/amt-4-717-2011, 2011.

Yoshida, Y., Kikuchi, N., Morino, I., Uchino, O., Oshchepkov, S., Bril, A., Saeki, T., Schutgens, N., Toon, G. C., Wunch, D., Roehl, C. M., Wennberg, P. O., Griffith, D. W. T., Deutscher, N. M., Warneke, T., Notholt, J., Robinson, J., Sherlock, V., Connor, B., Rettinger, M., Sussmann, R., Ahonen, P., Heikkinen, P., Kyrö, E., Mendonca, J., Strong, K., Hase, F., Dohe, S., and Yokota, T.: Improvement of the retrieval algorithm for GOSAT SWIR XCO_2 and XCH_4 and their validation using TCCON data, Atmos. Meas. Tech., 6, 1533–1547, doi:10.5194/amt-6-1533-2013, 2013.